

Models of wave supported clumps in giant molecular clouds

R.F. Coker, J.G.L. Rae, and T.W. Hartquist

University of Leeds, Department of Physics and Astronomy, Leeds LS2 9JT, UK
(robc@ast.leeds.ac.uk; jglr@ast.leeds.ac.uk; twh@ast.leeds.ac.uk)

Received 29 February 2000 / Accepted 24 May 2000

Abstract. We present plane-parallel equilibrium models of molecular clumps that are supported by Alfvén waves damped by the linear process of ion-neutral friction. We used a WKB approximation to treat the inward propagation of waves and adopted a realistic ionization structure influenced by dissociation and ionization due to photons of external origin. The model clumps contain central condensations surrounded by lower density envelopes and are more condensed than those obtained for an assumed ionization structure, used in some previous studies, that is more appropriate for dark regions. In some parameter regimes the structures of clumps depend sensitively on the assumed depletions of Sulphur and metals.

Key words: ISM: clouds – ISM: magnetic fields – turbulence – waves

1. Introduction

Giant molecular cloud complexes (GMCs), the birth places of stars, are typically many tens of parsecs in linear extent and have masses from 10^4 to $10^6 M_{\odot}$ and temperatures of 10–30 K (see Hartquist et al. 1998 for a recent review). Observations of CO emission from GMCs (Blitz & Thaddeus 1980; Williams et al. 1995) show them to be composed of many smaller clumps that are a few parsecs in extent and contain $\lesssim 10^3 M_{\odot}$.

The widths of CO emission lines originating in individual clumps are supersonic and have been attributed to the presence of Alfvén waves having subAlfvénic velocity amplitudes (Arons & Max 1975). The Alfvén waves contribute to the support of a clump along the direction of the large-scale magnetic field (e.g., Fatuzzo & Adams 1993); the damping of the waves affects the degree of support that they provide. An important and well understood mechanism for the damping of linear Alfvén waves in a partially ionized medium is that due to ion-neutral friction which depends on the ionization structure (Kulsrud & Pearce 1969). Ruffle et al. (1998, hereafter R98) and Hartquist et al. (1993) have emphasised that the dependence of the ionization structure on total visual extinction, A_V , should greatly influence the density profiles of clumps if Alfvén waves

contribute to their support. To quantify the assertion of Hartquist et al. (1993) and R98, we present in this paper models of plane-parallel, wave-supported GMC clumps like those identified in the work of Williams et al. (1995), who made a detailed analysis of the CO maps of the Rosette Molecular Cloud (RMC), identifying more than 70 clumps. The models that we have constructed are for RMC-type clumps in equilibrium, a restriction justified by the fact that clear spectral signatures of collapse have been found only when much smaller scale features have been resolved (see, e.g., Hartquist et al. 1998).

We have adopted a WKB description of the wave propagation as did Martin et al. (1997) in their work on wave-supported clumps. Their work differs substantially from ours in that they used an ionization structure appropriate for dark regions. Also, we have considered inwardly rather than outwardly propagating waves, as many of the clumps mapped by Williams et al. (1995) do not contain detected stars and may have no internal means of generating waves. Indeed, the waves may be produced at the surface of a clump by its interaction with an interclump medium.

Other authors have addressed the importance of photoabsorption for the effects that the ionization structure will have upon a clump’s dynamics. These authors have been concerned primarily with dense cores and/or envelopes around them; cores are much smaller-scale objects than the clumps identified in Williams et al. (1995). McKee (1989) addressed the possibility that collapse in a system of dense cores is a self-regulating process due to the ionization of metals such as Magnesium and Sodium by photons emitted by stars formed in the collapse; he was concerned with infall due to ambipolar diffusion of a large-scale magnetic field. Ciolek & Mouschovias (1995) have shown that the large-scale magnetic field can support a photoionized envelope around a dense core for a time that is very long compared to the ambipolar diffusion timescale in the centre of the dense core. In contrast to McKee (1989) and Ciolek & Mouschovias (1995), Myers & Lazarian (1998) addressed the effect of photoabsorption on support by waves rather than by the large-scale magnetic field. They stressed that observed infall of dense core envelopes is slower than that expected due to gravitational free-fall and more rapid than collapse due to the reduction by ambipolar diffusion of support by an ordered large-scale magnetic field. They considered collapse of mate-

rial supported primarily by waves and subjected to an external radiation field. While they made clear comments about the importance of the A_V dependence of the ionization structure for their model, they did not perform any detailed calculations in which a realistic dependence of the ionization fraction on A_V was used.

Several sets of authors have considered nonlinear effects in the dissipation of waves supporting a clump. Gammie & Ostriker (1996) investigated models of plane-parallel clumps and from their “1 2/3-dimensional” models found dissipation times due to nonlinear effects to be longer than the Alfvén crossing times for a fairly large range of parameters. They state that insofar as their models allow for compressibility, but not a perpendicular Alfvén-wave cascade, their work is complementary to that of Sridhar & Goldreich (1994); the same is true for the work presented here. The three dimensional investigations of Mac Low et al. (1998) and Stone et al. (1998) suggest the more restrictive condition that the angular frequency of the longest waves be no more than a few times $2\pi/t_A$ (where t_A is the Alfvén crossing time) in order for the dissipation timescale due to nonlinear damping to be roughly the Alfvén crossing time or more. In this paper we have restricted our attention to such angular frequencies so that we are justified to lowest order in focusing on only the damping due to ion-neutral friction. It should be noted that the above three dimensional studies of nonlinear effects concerned homogeneous turbulence and did not include ion-neutral damping for a realistic ionization structure. If we are correct in supposing that the waves in clumps are driven externally, then the turbulence is not homogeneous and its nature depends on both the viscous scale set by ion-neutral damping and the exact boundary conditions. The effects of nonlinear damping and multiple dimensions will be considered in subsequent work.

In Sect. 2 we present the equations for the wave energy, the static equilibrium clump structure, and the gravitational field. In Sect. 3 we give a description of the calculations of the ionization structure for various values of the clump density and A_V while Sect. 4 contains details of the models considered here. Finally, in Sect. 5, we present conclusions.

2. Equations of wave propagation and static equilibrium

We consider plane-parallel clumps with $z = 0$ corresponding to the clump midplane and $z = z_b$ (with z_b defined as positive) corresponding to boundary between the clump and the inter-clump medium. The large-scale magnetic field is taken to be $B_0\hat{z}$ with \hat{z} normal to the surface of a plane-parallel clump. We study waves of angular frequency ω propagating from $z = \pm z_b$ in the $\mp\hat{z}$ direction. Without loss of generality we shall assume that the perturbation magnetic field and velocity are in the \hat{x} direction.

Following the work of Hartquist & Morfill (1984, hereafter HM84), the ion velocity can be expressed as

$$v_i\hat{x} = v_o\hat{x}e^{\int k_i dz}e^{-i\int k_r dz}, \quad (1)$$

where v_o is a complex constant and k_r and k_i are the real and imaginary components, respectively, of the complex wave vector. The Appendix summarizes arguments used by HM84 to show that for an inwardly propagating linear Alfvén wave

$$\frac{d}{dz}(k_r v_i v_i^*) = \frac{V_2}{v_{A_i}^2} v_i v_i^*, \quad (2)$$

where v_i^* is the complex conjugate of v_i and

$$V_2 \equiv \frac{\nu_0 \omega^3 \rho_n^2}{\nu_0^2 \rho_i^2 + \omega^2 \rho_n^2}, \quad (3)$$

where ρ_i is ion mass density and ρ_n is the neutral mass density. The ion Alfvén speed is given by

$$v_{A_i} = \frac{B_0}{\sqrt{4\pi\rho_i}}. \quad (4)$$

The ion-neutral coupling frequency, ν_0 , is such that the momentum transfer per unit volume per unit time from ions to neutrals is given by $\nu_0\rho_i(v_i - v_n)\hat{x}$ where $v_n\hat{x}$ is the velocity of the neutrals. To a reasonably good approximation, C^+ is the dominant ion and, assuming cosmic abundances, we may take

$$\nu_0\rho_i \simeq 1.3 \times 10^{-9} \text{ s}^{-1} \left(\frac{n_i}{1 \text{ cm}^{-3}} \right) \rho_n \quad (5)$$

where n_i is the ion number density (Osterbrock 1961). If the dominant ion species are very massive, the constant would approach $1.6 \times 10^{-9} \text{ s}^{-1}$. However, in this work we ignore this dependence and use $12 m_H$ as the mass per ion.

Use of Eqs. (1), (2), and (A.3) yields

$$\frac{d}{dz} \left(\frac{k_r}{k_r^2 + k_i^2} b b^* \right) = \frac{V_2}{v_{A_i}^2} \frac{b b^*}{k_r^2 + k_i^2}, \quad (6)$$

where $b\hat{x}$ is the perturbation magnetic field and $b^*\hat{x}$ is its complex conjugate. In the WKB approximation,

$$\frac{d^2}{dz^2} e^{\int k_i dz} \simeq 0, \quad (7)$$

which is equivalent to assuming

$$|dk_i/dz - k_i^2| \ll k_r^2. \quad (8)$$

Then it follows (cf. Eq. A.5) that in the WKB approximation

$$k_r^2 \simeq \frac{\omega^2 + V_1}{v_{A_i}^2}, \quad (9)$$

with

$$V_1 \equiv \frac{\nu_0^2 \omega^2 \rho_n \rho_i}{\nu_0^2 \rho_i^2 + \omega^2 \rho_n^2}. \quad (10)$$

Similarity (cf. Eq. A.6), we take

$$k_i^2 \simeq \frac{V_2^2}{4(\omega^2 + V_1)v_{A_i}^2} \quad (11)$$

and substitute Eqs. (9) and (11) into Eq. (6) to find

$$\frac{d}{dz} \left(\frac{(\omega^2 + V_1)^{3/2} v_{A_i} U}{(\omega^2 + V_1)^2 + V_2^2/4} \right) = \frac{V_2(\omega^2 + V_1)}{(\omega^2 + V_1)^2 + V_2^2/4} U, \quad (12)$$

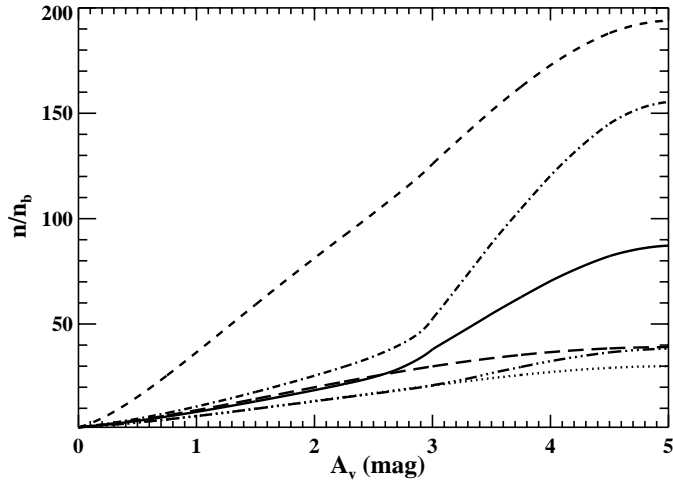


Fig. 1. Plot of density (normalized to the density at the outer edge of the clump) versus A_V for all Models. The solid curve is for Model 1, the dotted curve for Model 2, the dash-chain-dot curve for Model 3, the dot-dashed curve for Model 4, the dashed curve for Model 5, and the long-dashed curve is for Model 6.

where $U = bb^*/16\pi$ is the time-averaged energy density of the perturbation magnetic field. For an upward propagating wave, the sign of the RHS in Eq. (12) is negative. Note that if $\omega^2 \ll V_1$ and dissipation is neglected, Eq. (12) shows that the wave pressure increases as $\sqrt{\rho_n + \rho_i}$. This is a result in agreement with the work of Fatuzzo & Adams (1993) and McKee & Zweibel (1995); such a polytropic dependence for the wave pressure has been assumed in recent work by McKee & Holliman (1999) on the structure of molecular clumps.

We solve Eq. (12) along with the static equilibrium equation

$$c_s^2 \frac{d(\rho_n + \rho_i)}{dz} + \frac{dU}{dz} = -(\rho_n + \rho_i)g \quad (13)$$

(Martin et al. 1997) and the gravitational equation

$$\frac{dg}{dz} = 4\pi G(\rho_n + \rho_i), \quad (14)$$

where c_s , g , and G are the isothermal sound speed, the strength of the gravitational field, and the gravitational constant, respectively.

We verify, a posteriori, that Eq. (8) is valid by checking that

$$\left| \frac{dk_i}{dz} - \frac{V_2^2}{4v_{A_i}^2(\omega^2 + V_1)} \right| \ll \frac{\omega^2 + V_1}{v_{A_i}^2} \quad (15)$$

(see also Eq. 19 below).

3. Calculations of the ionization structure

The ionization structure determined by R98 and presented in their Fig. 1 was calculated on the assumption that, due to shielding of the CO by itself and by H_2 , the rate of CO dissociation by photons of external origin is negligible. For a plane-parallel semi-infinite cloud with constant Hydrogen nucleus number density, $n_H = 10^3 \text{ cm}^{-3}$, we assume an A_V -dependent dissociation rate that results in a CO abundance relative to n_H ,

Table 1. Assumed CO Photodissociation Rates

A_V	Rate (s^{-1})	$x(\text{CO})$
0.5	7.685×10^{-13}	9.132×10^{-7}
1.0	4.279×10^{-13}	2.248×10^{-6}
1.5	2.132×10^{-13}	5.248×10^{-6}
1.75	1.440×10^{-13}	7.538×10^{-6}
2.0	7.465×10^{-14}	1.226×10^{-5}
2.25	4.864×10^{-14}	1.503×10^{-5}
2.5	2.245×10^{-14}	2.166×10^{-5}
2.75	1.405×10^{-14}	2.381×10^{-5}
3.0	4.291×10^{-15}	3.621×10^{-5}
3.25	4.112×10^{-15}	3.620×10^{-5}
3.5	3.669×10^{-16}	6.336×10^{-5}
3.75	1.200×10^{-16}	8.976×10^{-5}
4.0	0	9.767×10^{-5}

Table 2. Fractional Elemental Abundances

	Case A	Case B
He	7×10^{-2}	7×10^{-2}
C	1×10^{-4}	1×10^{-4}
O	2×10^{-4}	2×10^{-4}
S	2×10^{-8}	3×10^{-6}
Na	2×10^{-7}	1×10^{-6}

$x(\text{CO})$, that is in harmony with the measurements shown in Fig. 6 of van Dishoeck (1998). For the $n_H = 10^3 \text{ cm}^{-3}$ model, Table 1 gives $x(\text{CO})$ and the photodissociation rate as a function of A_V . Note that the total abundance of carbon nuclei relative to n_H is fixed at 10^{-4} . In the work reported here, we used an ionization fraction that depends on both A_V and n_H . Using the A_V -dependent CO photodissociation rate from Table 1, we calculated the fractional ionization as a function of A_V for $n_H = 3 \times 10^2, 3 \times 10^3$, and 10^4 cm^{-3} at various A_V values. A bilinear interpolation in A_V and n_H is used to find the actual ionization fraction used for a given point in the clump. For densities above 10^4 cm^{-3} we assume that the total ionization fraction, $\xi \equiv \rho_i/\rho_n$, goes as $n_H^{-1/2}$, as expected in a dark region. Note that in all models, when A_V is greater than 4, $n_H \gtrsim 10^4 \text{ cm}^{-3}$.

Since the depletions in RMC-type clumps are very uncertain, we present results for both depletion cases given in R98. As discussed therein (also see Shalabiea & Greenberg 1995), case A abundances resemble those seen in dark cores with centre-to-edge $A_V \gtrsim 5$ while case B, with higher fractional abundances of lower ionization potential elements, is more appropriate for more diffuse clouds. The fractional elemental abundances relative to n_H for case A and case B are given in Table 2.

4. Details of the models

Many RMC-type clumps are not bound by their own gravity and must be confined by interclump media (Bertoldi & McKee 1992). However, we shall assume that the interclump medium is sufficiently tenuous that it does not shield the clump from the standard interstellar background

radiation field used in the calculation of ξ so that $A_V = 0$ at $z = z_b$. The material on either side of the interface between a clump and the interclump medium is in two distinct phases, and we may assume that at its outer boundary a clump has a substantial density; we take $n(\text{H}_2) = n_{\text{H}}/2$ everywhere in the clump. Waves may exist in the interclump medium and be partially transmitted into the clump, or, as mentioned earlier, may be generated near the interface by the interaction between the clump and the interclump medium. Consequently, we assume that the magnitude of the amplitude of the perturbation magnetic field, $\delta B = \sqrt{bb^*}$, is, at $z = z_b$, a substantial fraction, f_b , of the large-scale field, B_0 .

In all models we have taken the mean mass per neutral particle, μ_n , to be 2.3 amu, corresponding to a cosmic abundance (Allen 1976) of 14% of the neutral particles being He and 86% being H_2 . Thus the number density of neutral particles at $z = z_b$, $n_b \equiv 0.58 n_{\text{H}}(z = z_b)$. As is consistent with data given by Savage & Mathis (1979), we have assumed

$$A_V = \frac{N_{\text{H}}}{1.9 \times 10^{21} \text{ cm}^{-2}}, \quad (16)$$

where N_{H} is the column density of Hydrogen nuclei. Also, the temperature throughout a clump was taken to be 20 K.

We assume that identical perturbations are generated at both interfaces of the plane-parallel clump (i.e. at z_b and $-z_b$), resulting in downward propagating waves (U_-) and upward propagating waves (U_+) which are assumed to be incoherent so that their contributions to the magnetic energy density are additive. Thus, Eq. (12) is actually solved as two separate equations. Also, in practice, we solve the problem in A_V -space (rather than z -space) by using the fact that

$$\frac{dA_V}{dz} = -C\rho. \quad (17)$$

With Eq. (16) and the distribution of neutral particles given above, $C \simeq 240 \text{ cm}^2 \text{ g}^{-1}$. Eq. (17) results in closed-form algebraic expressions for ρ and g , leaving only Eq. (12) to be evaluated. For a given setup, with $h \equiv U_+/U_-$, an initial boundary value of $h(z = z_b) \equiv h_b$, was selected and Eq. (12) was numerically integrated using an adaptive Gear algorithm (Gear 1971). The value of h_b was changed by iteration until the inner boundary condition $U_+(z = 0) = U_-(z = 0)$ was satisfied.

We have considered other models but present full results only for models which have a total edge-to-centre visual extinction of 5 magnitudes since, as discussed in R98, it is in the region of A_V of a few that clumps appear to begin to contain detected stars, while many dense cores may have $A_V \lesssim 5$ (McKee 1989).

We require a velocity amplitude,

$$V = 2\sqrt{\frac{U_+ + U_-}{\rho}}, \quad (18)$$

of 2 km s^{-1} and an Alfvén speed, v_A , of 3 km s^{-1} at $A_V = 2$. Since the concentration of CO at $A_V \lesssim 2$ is very low and measurements of GMC clump CO profiles have a width of $\sim 2 \text{ km s}^{-1}$ (Williams et al. 1995), observations require such velocities

Table 3. Summary of Models

#	$\omega \text{ (s}^{-1}\text{)}$	$n_b \text{ (cm}^{-3}\text{)}$	$B_0 \text{ (}\mu\text{G)}$	$z_b \text{ (pc)}$	Case
1	2×10^{-12}	200	127	0.84	A
2	2×10^{-12}	200	127	1.10	B
3	1×10^{-12}	200	127	1.08	A
4	2×10^{-12}	100	127	1.37	A
5	2×10^{-12}	200	63	0.31	A
6	5.5×10^{-13}	200	127	0.84	— ^a

^a Uses Eq. (20).

to exist well within the cloud. Also, we use a wave frequency, ω , of $2 \times 10^{-12} \text{ s}^{-1}$; this results in relatively strong neutral-ion coupling while keeping the wavelength of the perturbing wave less than the total size of the cloud. In other words,

$$\nu_0 \xi > \omega > \frac{2\pi}{\int dz/v_A}, \quad (19)$$

with $v_A \equiv \omega v_{A_i} / \sqrt{\omega^2 + V_1^2}$. Within the above constraints and given a boundary density $n_b = 200 \text{ cm}^{-3}$, we find for our canonical model (Model 1) the solution permitting the smallest value of B_0 (and correspondingly largest value of f_b) for which $V < v_A$ everywhere in the clump. We find that in order to satisfy all of the above constraints, we require $B_0 = 127 \mu\text{G}$ and $f_b = 0.323$.

We present results for 6 models. Model 1 is for the above canonical parameters with R98's depletion case A while Model 2 is for case B. Model 3 is the same as Model 1 but with $\omega = 1 \times 10^{-12}$ to illustrate the effect of a scenario with roughly maximum ion-neutral coupling. Model 4 has $n_b = 100 \text{ cm}^{-3}$ while Model 5 has $B_0 = 63 \mu\text{G}$. Model 6 has an ionization profile given by

$$\xi = 3 \times 10^{-16} \left(\frac{\rho_n}{\text{g cm}^{-3}} \right)^{-1/2} \quad (20)$$

(see, e.g., McKee 1989 and Myers & Lazarian 1998) and the largest possible value of ω which satisfies Eq. (19). Thus, Model 6 is for a dark region surrounded by interclump material. A summary of the parameters of the 6 models is given in Table 3. For all models, $f_b = 0.323$. For comparison, note that a waveless clump (i.e. $f_b = 0$) has a size of $z_b = 0.09 \text{ pc}$ and a central density enhancement of more than 300.

5. Results and conclusions

In Fig. 1 we present density as a function of visual extinction for each of the 6 Models. The ionization structures influenced by photons of external origin can result in more extended clumps (e.g. Model 3) with flatter envelope density profiles than the ionization profile used in Model 6. The weaker large-scale field of Model 5 results in little wave support so the clump's density profile approaches that of a thermally supported cloud.

In Fig. 2 we show plots of δB versus A_V for the downward propagating wave for all Models. Except for Model 6, which has $k_i/k_T \sim 1$ at the clump boundary, the perturbing field obeys flux

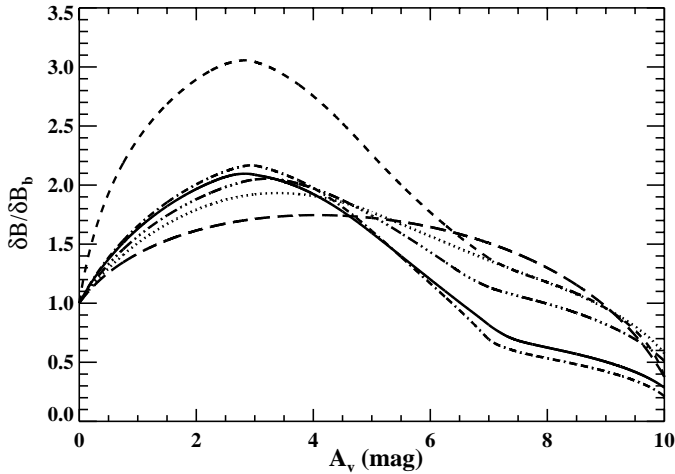


Fig. 2. As Fig. 1 but for the downward propagating perturbing magnetic field, δB . Here, $A_V > 5$ corresponds to $z < 0$.

conservation near the surface of the clump. In the central regions of Models 1 and 4, dissipation is rapid enough that δB begins to significantly decrease before reaching the clump centre. In order to compensate for the loss of wave support, the equilibrium solution requires a complementary increase in the density, as can be seen in Fig. 1. On the other hand, in Model 6, the wave is dissipated only close to the cloud boundary, permitting a flat density profile. Similarly, the higher ionization fractions of the case B depletions result in very little dissipation even in the centre of the clump for Model 2. Note that even though observations (Williams et al. 1995) suggest that the temperature of RMC-type clumps is closer to 10 K rather than the 20 K used here, thermal support is in general unimportant, so the effect of a lower temperature on the models would be to enhance slightly any central condensations.

The ionization profiles used in the Models are shown in Fig. 3. The ionization profiles described in Sect. 3 result in ξ for Models 1–5 being ~ 100 times greater near the surface of the clump than in Model 6. This leads to larger clumps which, if there is significant dissipation in the centre, also have small condensed cores. Clumps with $A_V \gtrsim 5$ are likely to have distinct central condensations with $n/n_b \gtrsim 50$ and central fractional ionizations of $\lesssim 5 \times 10^{-7}$. Though dense cores may be formed during the fairly rapid collapse (as envisaged by Fielder & Mouschovias 1993) of more extended objects (i.e. RMC-like clumps) that become unstable, even in our equilibrium models we find central cores having densities and fractional ionizations similar to those measured for dense cores and their envelopes (Williams et al. 1995; Williams et al. 1998; Bergin et al. 1999).

Fig. 4 shows the flux of magnetic energy through the clumps for Models 1–6. In Models 1 and 4 the dissipation is sufficient for thermal pressure to contribute nonnegligibly to the support near the clump centres. The higher ionization fraction for the case B depletions used in Model 2 results in less dissipation and thus more wave support for the clump. Consequently, as can be seen in Fig. 1, Model 2 has no central condensation and is more

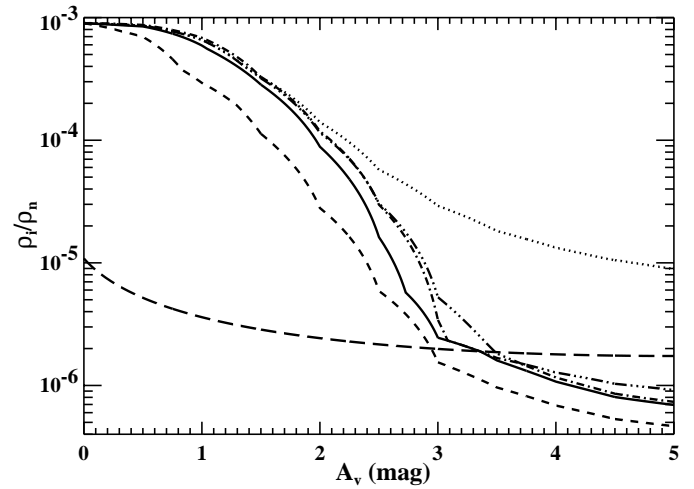


Fig. 3. As Fig. 1 but for the absolute ion mass fraction, ξ . The bumps seen on the curves for Models 1–5 are a result of the interpolation over A_V .

extended. Unfortunately, we can only speculate about how the depletions of Sulphur, metals, and some other species behave in RMC-like clumps (Ruffle et al. 1999). Thus, cases A and B are merely representative; as can be clearly seen in the figures, the clump profiles are very sensitive to the choice of abundances and the subsequent fractional ionizations. In addition, compared to Model 1, the stronger ion-neutral coupling in Model 3 results in less dissipation and subsequently the clump has little central condensation, as expected.

Fig. 4 also shows the effect of external wave generation. If the fractional ionization is too low, as in Model 6, dissipation occurs close to the surface of the clump. Conversely, if the fractional ionization is too large, as in Model 2, significant dissipation occurs only at the clump's very centre (if at all). Both extremes produce clumps with density profiles which lack a central condensation. Note that if our externally generated wave model is correct, one should not see turbulence within a condensed cloud if there is no turbulence in its surrounding envelope.

In Fig. 5 we present curves which map the visual extinction to the spatial extent of the clumps. Within the constraints given in Sect. 4, most of the Models have extents ($= 2 \times z_b$) which match the observed ~ 2 pc size of RMC-type clumps (Williams et al. 1995). However, models with a weak large-scale magnetic field (e.g. Model 5) produce clumps which are less than a parsec in size. Note, however, that observations generally measure the largest linear extent of a clump and the waves only support the model clumps parallel to the large-scale field.

The models require high densities and large magnetic field strengths in order for the Alfvén speed and wave velocity amplitude at visual extinctions where CO is abundant to be large enough to be compatible with observed line-widths. For most of the models presented here, $n_b = 200 \text{ cm}^{-3}$. This results in a density at $A_V = 2$ of $\gtrsim 2500 \text{ cm}^{-3}$, rather higher than the typical values which are within a factor of about 4 of 250 cm^{-3} (Williams et al. 1995) for RMC-type clumps but, given the con-

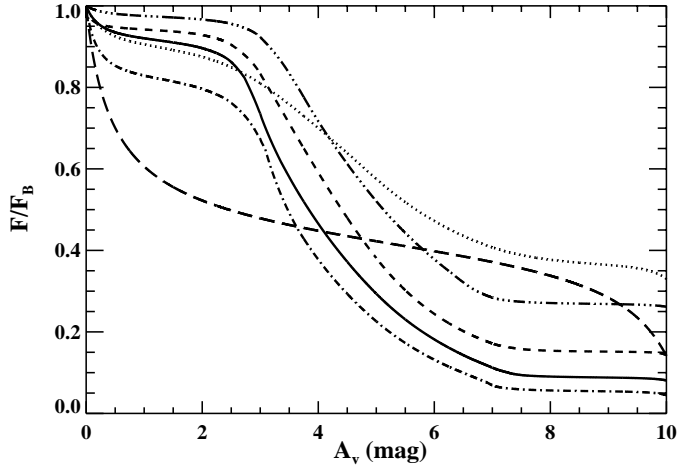


Fig. 4. As Fig. 1 but for the magnetic energy flux ($F \equiv k_r U \omega / |k|^2$) of the downward propagating Alfvén wave. Here, $A_V > 5$ corresponds to $z < 0$.

siderable uncertainties, it is within a reasonable range of the Williams et al. (1995) values. The models given here also require $B_0 = 127 \mu\text{G}$; this is significantly higher than the value of $30 \mu\text{G}$ suggested by observations (Heiles 1987) and expected from robust theoretical arguments (Mouschovias 1987). In order to determine whether the values of $n(A_V = 2)$ and B_0 could be lower and still allow model properties to be consistent with observed linewidths, we constructed models for clumps with edge-to-centre extinctions of 3 magnitudes. The model with $n_b = 200 \text{ cm}^{-3}$ which gave $V = 2 \text{ km sec}^{-1}$ and $v_A = 3 \text{ km sec}^{-1}$ at $A_V = 2$, had $B_0 = 95 \mu\text{G}$, $f_b = 0.331$, and $n(A_V = 2) \sim 2000 \text{ cm}^{-3}$. In general, if the conditions discussed in Sect. 4 on V and v_A are met, the value of $n(A_V = 2)$ is not very sensitive to n_b .

Thus, the next step in the modelling of self-gravitating clumps in which wave support is important is the inclusion of wave support in models analogous to the axisymmetric models of magnetically and thermally supported clumps described in classic papers by Mouschovias (1976a,b). It is possible that the inclusion of magnetic tension, as well as pressure, will allow the reduction of B_0 to a value more like that expected.

Acknowledgements. This work was supported by PPARC and has made use of NASA's Astrophysics Data System Abstract Service. We thank an anonymous referee whose comments led to improvement and further extension of the work and Chris McKee for pointing out some additional references.

Appendix: two-fluid linear treatment of Alfvén waves

The linearized equations of motion for the Alfvén waves are

$$\rho_n \frac{\partial v_n}{\partial t} = \nu_0 \rho_i (v_i - v_n) \quad (\text{A.1})$$

$$\rho_i \frac{\partial v_i}{\partial t} = -\nu_0 \rho_i (v_i - v_n) + \frac{B_0}{4\pi} \frac{\partial b}{\partial z} \quad (\text{A.2})$$

$$\frac{\partial b}{\partial t} = B_0 \frac{\partial v_i}{\partial z} \quad (\text{A.3})$$

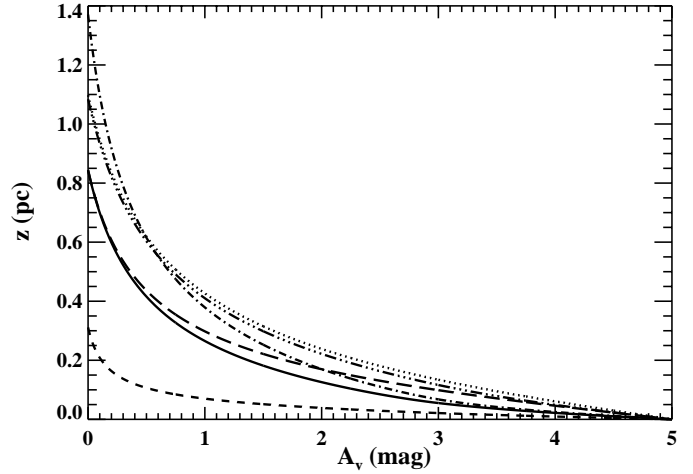


Fig. 5. As Fig. 1 but for z , the absolute spatial extent of the plane-parallel cloud.

If we take a solution that depends on time as $e^{i\omega t}$, we can use Eqs. (A.1)–(A.3) to find that

$$(\omega^2 + V_1 + iV_2)v_i = -\frac{B_0^2}{4\pi} \frac{\partial^2 v_i}{\partial z^2}, \quad (\text{A.4})$$

where V_1 and V_2 are given by Eqs. (10) and (4) respectively. Following HM84, we multiply Eq. (A.4) by v_i^* and the complex conjugate of Eq. (A.4) by v_i and subtract and then use Eq. (1) to find Eq. (2). Substitution of Eq. (1) in Eq. (A.4) yields

$$\frac{\omega^2 + V_1}{v_{A_i}^2} = k_r^2 - k_i^2 + \frac{dk_i}{dz} \quad (\text{A.5})$$

and

$$\frac{V_2}{v_{A_i}^2} = \frac{dk_r}{dz} - 2k_r k_i. \quad (\text{A.6})$$

References

- Allen C.W., 1976, *Astrophysical Quantities*. Athlone Press, London
- Arons J., Max C.E., 1975, *ApJ* 196, L77
- Bergin E.A., Plume R., Williams J.P., Myers P.C., 1999, *ApJ* 512, 724
- Bertoldi F., McKee C.F., 1992, *ApJ* 395, 140
- Blitz L., Thaddeus P., 1980, *ApJ* 241, 676
- Ciolek G.E., Mouschovias T.Ch., 1995, *ApJ* 454, 194
- Fatuzzo M., Adams F.C., 1993, *ApJ* 412, 46
- Fiedler R.A., Mouschovias T.Ch., 1993, *ApJ* 415, 680
- Gammie C.F., Ostriker E.C., 1996, *ApJ* 466, 814
- Gear C.W., 1971, *Prentice-Hall Series in Automatic Computation*, Prentice-Hall, Englewood Cliffs
- Hartquist T.W., Morfill G.E., 1984, *ApJ* 287, 194 (HM84)
- Hartquist T.W., Rawlings J.M.C., Williams D.A., Dalgarno A., 1993, *QJRAS* 34, 213
- Hartquist T.W., Caselli P., Rawlings J.M.C., Ruffle D.P., Williams D.A., 1998, In: Hartquist T.W., Williams D.A. (eds.) *The Molecular Astrophysics of Stars and Galaxies*. Clarendon Press, Oxford, p. 101
- Heiles C., 1987, In: Hollenbach D.J., Thronson H.A. (eds.) *Interstellar Processes*. Reidel, Dordrecht, p. 171

- Kulsrud R., Pearce W.P., 1969, ApJ 156, 445
Mac Low M.-M., Klessen R.S., Burkert A., Smith M.D., 1998, Physical Review Letters 80, 2754
Martin C.E., Heyvaerts J., Priest E.R., 1997, A&A 326, 1176
McKee C.F., 1989, ApJ 345, 782
McKee C.F., Holliman J.H., 1999, ApJ 522, 313
McKee C.F., Zweibel E.G., 1995, ApJ 440, 686
Mouschovias T.Ch., 1976a, ApJ 206, 753
Mouschovias T.Ch., 1976b, ApJ 207, 141
Mouschovias T.Ch., 1987, In: Morfill G.E., Scholer M. (eds.) Physical Processes in Interstellar Clouds. p. 453
Myers P.C., Lazarian A., 1998, ApJ 507, L157
Osterbrock D.E., 1961, ApJ 134, 270
Ruffle D.P., Hartquist T.W., Rawlings J.M.C., Williams D.A., 1998, A&A 334, 678 (R98)
Ruffle D.P., Hartquist T.W., Caselli P., Williams D.A., 1999, MNRAS 306, 691
Savage B.D., Mathis J.S., 1979, ARA&A 17, 73
Shalabiea O.M., Greenberg J.M., 1995, A&A 296, 779
Sridhar S., Goldreich P., 1994, ApJ 432, 612
Stone J.M., Ostriker E.C., Gammie C.F., 1998, ApJ 508, L99
van Dishoeck E.F., 1998, In: Hartquist T.W., Williams D.A. (eds.) The Molecular Astrophysics of Stars and Galaxies. Clarendon Press, Oxford, p. 53
Williams J.P., Blitz L., Stark A.A., 1995, ApJ 451, 252
Williams J.P., Bergin E.A., Caselli P., Myers P.C., Plume R., 1998, ApJ 503, 689